Thyroid hormone is required for hypothalamic neurons regulating cardiovascular functions

Jens Mittag,[1] David J. Lyons,[2] Johan Sällström,[3] Milica Vujovic,[1] Susi Dudazy-Gralla,[1] Amy Warner,[1] Karin Wallis,[1] Anneke Alkemade,[4] Kristina Nordström,[1] Hannah Monyer,[5] Christian Broberger,[2] Anders Arner,[3] and Björn Vennström[1]

[1]Department of Cell and Molecular Biology, [2]Department of Neuroscience, and [3]Department of Physiology and Pharmacology, Karolinska Institutet, Stockholm, Sweden. [4]Alan Turing Institute Almere, Almere, The Netherlands. [5]Clinical Neurobiology, Universitätsklinikum Heidelberg, Heidelberg, Germany.

Thyroid hormone is well known for its profound direct effects on cardiovascular function and metabolism. Recent evidence, however, suggests that the hormone also regulates these systems indirectly through the central nervous system. While some of the molecular mechanisms underlying the hormone's central control of metabolism have been identified, its actions in the central cardiovascular control have remained enigmatic. Here, we describe a previously unknown population of parvalbuminergic neurons in the anterior hypothalamus that requires thyroid hormone receptor signaling for proper development. Specific stereotaxic ablation of these cells in the mouse resulted in hypertension and temperature-dependent tachycardia, indicating a role in the central autonomic control of blood pressure and heart rate. Moreover, the neurons exhibited intrinsic temperature sensitivity in patch-clamping experiments, providing a new connection between cardiovascular function and core temperature. Thus, the data identify what we believe to be a novel hypothalamic cell population potentially important for understanding hypertension and indicate developmental hypothyroidism as an epigenetic risk factor for cardiovascular disorders. Furthermore, the findings may be beneficial for treatment of the recently identified patients that have a mutation in thyroid hormone receptor α1.

Introduction

Thyroid hormone is a well-known regulator of cardiovascular function and metabolic rate (1, 2). Hyperthyroid patients display increased metabolic rate and weight loss, despite increased food intake, as well as a profound tachycardia (2). Conversely, hypothyroid patients often suffer from weight gain and bradycardia (3). While most of the cardiovascular and metabolic effects of thyroid hormone have been attributed to direct actions in the corresponding peripheral tissues, such as heart (4) or skeletal muscle and fat (5, 6), recent studies have demonstrated that the hormone modulates these processes also through the brain (7): injections of thyroid hormone into different brain regions stimulate energy expenditure (8), and thyroid hormone signaling is required to establish the metabolic set point during embryonal development (9, 10).

Similarly, thyroid hormone signaling is needed for the central modulation of heart rate. Mice that are heterozygous for a point mutation in thyroid hormone receptor α1 (*Thra1*$^{+/m}$), which reduces the affinity to the ligand 10 fold (11), were unable to mount a correct cardiovascular response to stress, activity, or changes in environmental temperature due to a defective autonomous nervous system (12). While progress has been made in unraveling the molecular mechanisms of action of thyroid hormone in the central metabolic control and the identification of the underlying neuroanatomical areas (13), little is known about the anatomical substrates that mediate the effects of thyroid hormone on cardiovascular function.

Here, we show that *Thra1*$^{+/m}$ mice exhibit fewer parvalbuminergic neurons in a previously unknown population in the anterior hypothalamic area (AHA). Stereotaxic ablation of these cells in parvalbumin (pv) Cre mice suggests a role in the central control of heart rate and blood pressure.

Conflict of interest: The authors have declared that no conflict of interest exists.
Citation for this article: *J Clin Invest.* 2013;123(1):509–516. doi:10.1172/JCI65252.

Results

Blood pressure regulation in Thra1$^{+/m}$ *mice*. The hypotension observed in the recently identified patient with a mutant thyroid hormone receptor α1 (TRα1) allele (14) prompted us to investigate blood pressure and associated serum parameters in our *Thra1*$^{+/m}$ animal model. Surprisingly, despite strongly reduced pulmonary angiotensin-converting enzyme (*Ace*) expression and lower serum angiotensin II levels in the mutant animals (Figure 1A), we found that blood pressure was similar to that in wild-type controls (Figure 1B). We thus tested whether the reduced *Ace* expression was an acute consequence of the defective TRα1 signaling by treating *Thra1*$^{+/m}$ mice with supraphysiological doses of triiodothyronine (T3), which reactivates signaling through the mutant receptor (11). The treatment increased pulmonary *Ace* expression, normalized serum angiotensin levels (Figure 1C), and restored the bradycardia in the mice (12). Determination of blood pressure in the T3-treated animals, which now had normalized heart rate and angiotensin II levels, revealed a 25% increase in systolic, diastolic, and mean arterial pressure (Figure 1D), suggesting an additional defect in the control of cardiovascular function in *Thra1*$^{+/m}$ mice. As the phenotype was only revealed in the T3-treated adult animal, we hypothesized that a developmental defect residing in the central nervous system caused this phenotype.

Fewer pv neurons in the anterior hypothalamus of Thra1$^{+/m}$ *mice*. Our previous studies already indicated a defect in the central autonomic control of cardiovascular function (12). Thus, we examined the cellular composition of the hypothalamus — the master regulator of the autonomic nervous system (15). The data revealed that the levels of pv mRNA were halved in the mutant animals (Supplemental Figure 1A; supplemental material available online with this article; doi:10.1172/JCI65252DS1). A subsequent immunohistochemical analysis identified an approximately 70% reduction of a previously unknown population of small hypothalamic pv^{+} cells (Figure 2, A and D) localized in the AHA (Supplemental Figure 1D). Cells

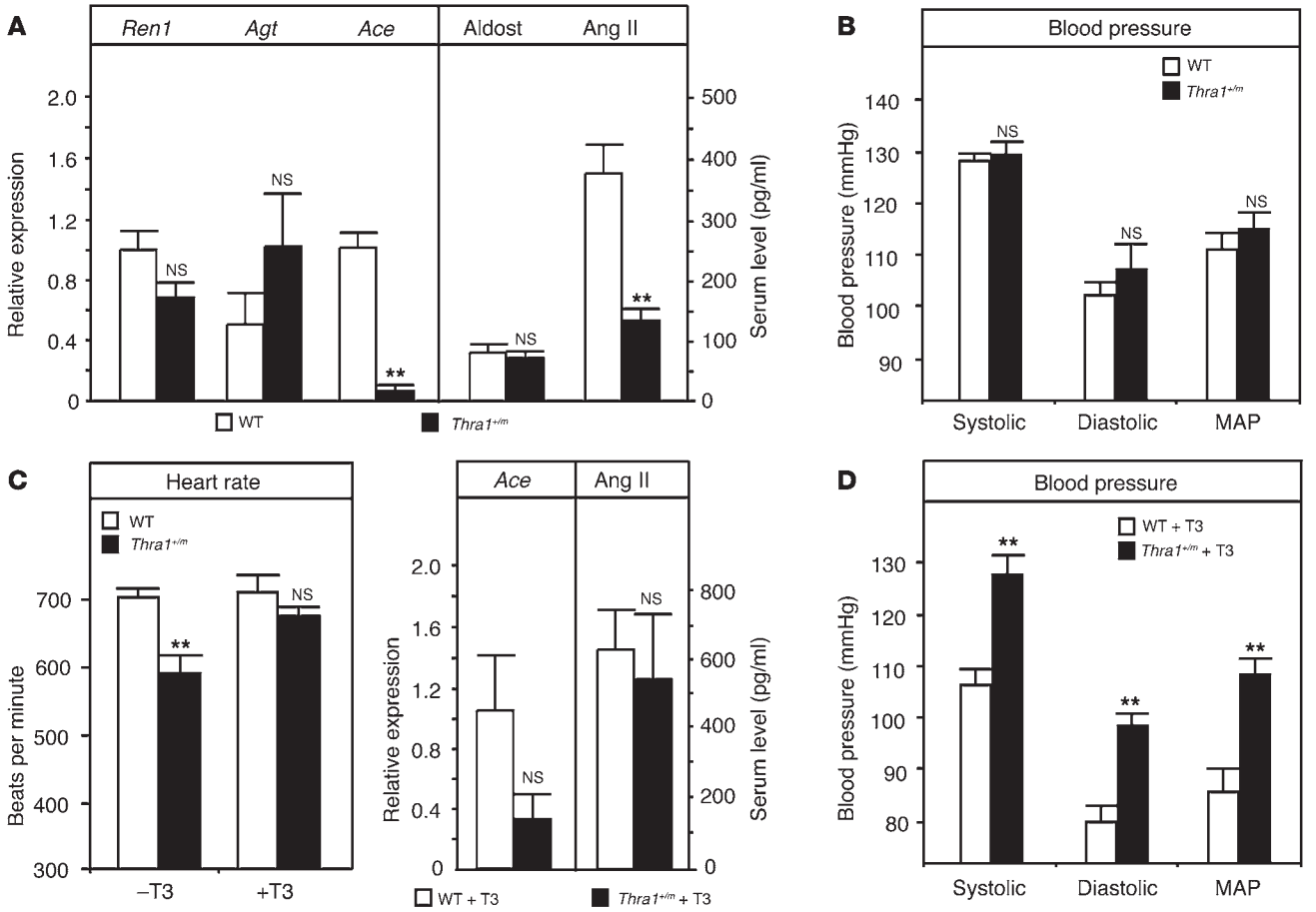

Figure 1

Regulation of blood pressure in *Thra1*$^{+/m}$ mice before and after treatment with T3. (**A**) mRNA expression of renal renin (*Ren1*), hepatic angiotensinogen (*Agt*), and pulmonary *Ace* as well as serum aldosterone (Aldost) and angiotensin II (Ang II) levels in wild-type and *Thra1*$^{+/m}$ mice. (**B**) Systolic, diastolic, and mean arterial blood pressure (MAP) in wild-type and *Thra1*$^{+/m}$ mice. (**C**) Heart rate in wild-type and *Thra1*$^{+/m}$ mice before and after T3 treatment as well as pulmonary *Ace* mRNA expression and serum angiotensin II levels in T3-treated animals. (**D**) Systolic, diastolic, and mean arterial blood pressure in T3-treated wild-type and *Thra1*$^{+/m}$ mice. All values are mean ± SEM; $n = 5$. $^{**}P < 0.01$. NS, not significant.

expressing other calcium-binding marker proteins, such as calretinin and calbindin, were unaffected (Supplemental Figure 1, A and B) as well as a more distant nucleus of pv$^+$ cells in the lateral hypothalamic area (Supplemental Figure 1B) described recently (16). Similar to pv$^+$ neurons in the cortex (17), the AHA pv$^+$ cells also appeared between postnatal days 7 and 14 (Supplemental Figure 1C).

As we detected the presence of TRα1 protein in the pv$^+$ cells (Figure 2B), we tested whether a reactivation of the mutant receptor through increased thyroid hormone levels (11) would restore the number of cells in *Thra1*$^{+/m}$ mice — either by a 14-day oral thyroid hormone treatment or through genetic inactivation of thyroid hormone receptor β (TRβ) that causes hyperthyroidism in the animals throughout their postnatal life (18). Neither condition led to normalization; in contrast, the lack of TR further reduced the number of cells in *Thra1*$^{+/m}$*Thrb*$^{-/-}$ and *Thra1*$^{+/+}$*Thrb*$^{-/-}$ animals (Figure 2, C and D). This observation demonstrates that intact thyroid hormone signalling via both TR isoforms is required for proper pv$^+$ cell development in the AHA and that the cells are absent in *Thra1*$^{+/m}$ mice rather than exhibiting a diminished pv expression due to impaired TRα1 signaling.

AHA pv$^+$ cells respond to temperature alterations and thyrotropin-releasing hormone stimulation. To obtain information on a possible function of the AHA pv$^+$ neurons, we performed whole-cell patch-clamp recordings (Figure 3A) in hypothalamic slices of adult mice expressing GFP under the pv promoter (19). While most of the cells were not responsive to angiotensin II (Figure 3B), all tested AHA pv$^+$ cells responded to alterations in temperature ranging from 25°C to 40°C. Sixty-nine percent of the cells were excited by increasing temperature with reversible depolarization and increase in action potential discharge, whereas 31% were inhibited and showed reversible hyperpolarization and cessation of action potential discharge (Figure 3C). This sensitivity persisted even after blocking synaptic transmission with tetrodotoxin, demonstrating that the thermosensitivity of pv$^+$ AHA neurons is an intrinsic property and not the consequence of other neuronal inputs (Supplemental Figure 2, A and B). No temperature sensitivity was observed in pv$^+$ neurons from the cortex in control experiments (Supplemental Figure 2B).

To reveal the underlying molecular mechanism, we performed voltage clamp ramps in the heat-inhibited neurons. These experiments revealed a current reversal at –85 mV (Supplemental Figure 2, C and D), which — in conjunction with the depolarizing effects of the potassium channel blocker tolbutamide (Supplemental Figure 2B) — suggested an involvement of K$^+$-ATP channel activation in

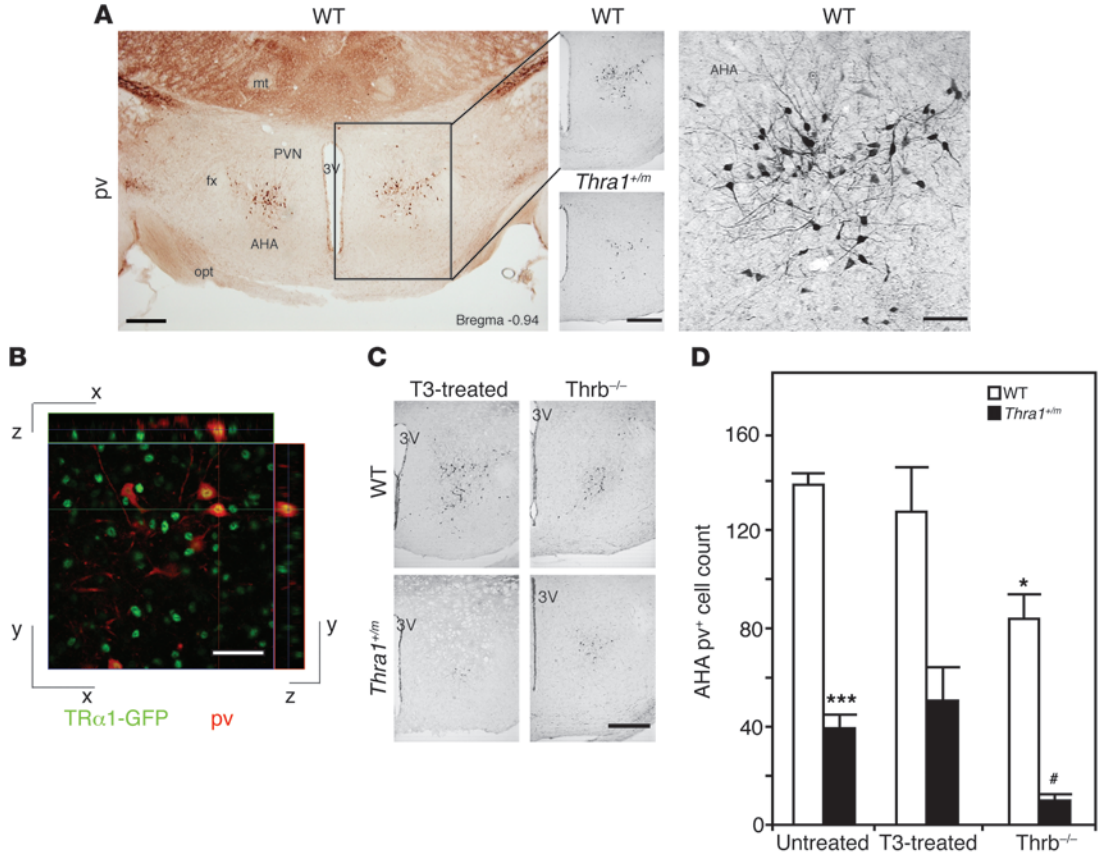

Figure 2

Reduced number of pv cells in the anterior hypothalamus of *Thra1*$^{+/m}$ mice. (**A**) Immunohistochemistry for pv in the anterior hypothalamus, as overview (left; scale bar: 250 μm) and high magnification (right; scale bar: 50 μm) in wild-type and *Thra1*$^{+/m}$ mice (middle; scale bar: 250 μm). fx, fornix; mt, mamillothalamic tract; PVN, paraventricular nucleus of the hypothalamus; 3V, 3rd ventricle; opt, optic tract. (**B**) Double immunohistochemistry for GFP (green) and pv (red) in the AHA of a mouse strain expressing a chimeric TRα1-GFP protein. Yellow indicates overlapping staining. Scale bar: 25 μm. (**C**) pv neurons in T3-treated wild-type and *Thra1*$^{+/m}$ mice or crossings with hyperthyroid *Thrb*$^{-/-}$ mice. Scale bar: 250 μm. (**D**) Quantification of pv neurons in the AHA of the different animal models. All values are mean ± SEM; $n = 4–9$. $^{*}P < 0.05$ to untreated wild type; $^{***}P < 0.001$ to untreated wild type; $^{\#}P < 0.05$ to untreated *Thra1*$^{+/m}$.

the thermosensation of these cells. We also detected the temperature-activated transient receptor potential (TRP) channel TRPV4 on 56% of the AHA pv^{+} cells (Supplemental Figure 2E), which likely contributes to the depolarization observed in the heat-excited pv^{+} cells (20, 21). That also TRPM8 was detected on a majority of AHA pv^{+} cells (Supplemental Figure 2E), indicates a complex interplay between several thermosensitive channels (22).

To differentiate better between the cell types, we tested whether other substances would also elicit different electrophysiological responses specific to some AHA pv^{+} neurons. Thyrotropin-releasing hormone (TRH), known to have central effects on the control of the autonomic nervous system (23–25), excited 48% (Figure 3D) and inhibited 19% of the neurons. Some of these inhibitions were associated with an increase in inhibitory postsynaptic potentials (Supplemental Figure 2, F and G), suggesting that the AHA pv^{+} neurons are part of a TRH excited inhibitory network. However, there was no correlation between the TRH response of a neuron and the type of temperature sensitivity, suggesting that at least 4 different subpopulations exist among the AHA pv^{+} neurons.

Physiological role of the pv^{+} cells in the AHA. To understand the physiological function of the pv^{+} neurons, we aimed to ablate the cells in vivo by stereotaxic injection of a novel conditionally neurotoxic adeno-associated virus (AAV) into the AHA of pvCre transgenic mice (Figure 4A). As a result of diphtheria toxin A expression after Cre recombination, we achieved approximately 40% reduction of pv^{+} cells in the AHA of pvCre mice (Figure 4C, right). The presence of GFP-positive cells at the injection site (Figure 4B) demonstrated that the infection was not lethal for Cre-negative cells. This was further corroborated by the absence of alterations in other hypothalamic cell populations of AAV-injected pvCre mice (Supplemental Figure 1E), including the pv^{+} cells in the lateral hypothalamus (16). Moreover, the number of pv^{+} cells in the AHA of AAV-injected wild-type mice remained normal as expected (Figure 4C, left).

Subsequent physiological analyses after the virus-induced ablations revealed no immediate effects on body weight, food intake, overall activity, respiratory quotient, or body temperature when compared to those of nonablated pvCre controls (Supplemental Figure 3, A–G). Furthermore, no activation of the brown fat was detected upon ablation (Supplemental Figure 3, H and I); only a minor decrease in oxygen consumption and carbon dioxide production was observed at room temperature (Supplemental Figure 3, D and E). In contrast, we found a prominent hypertension

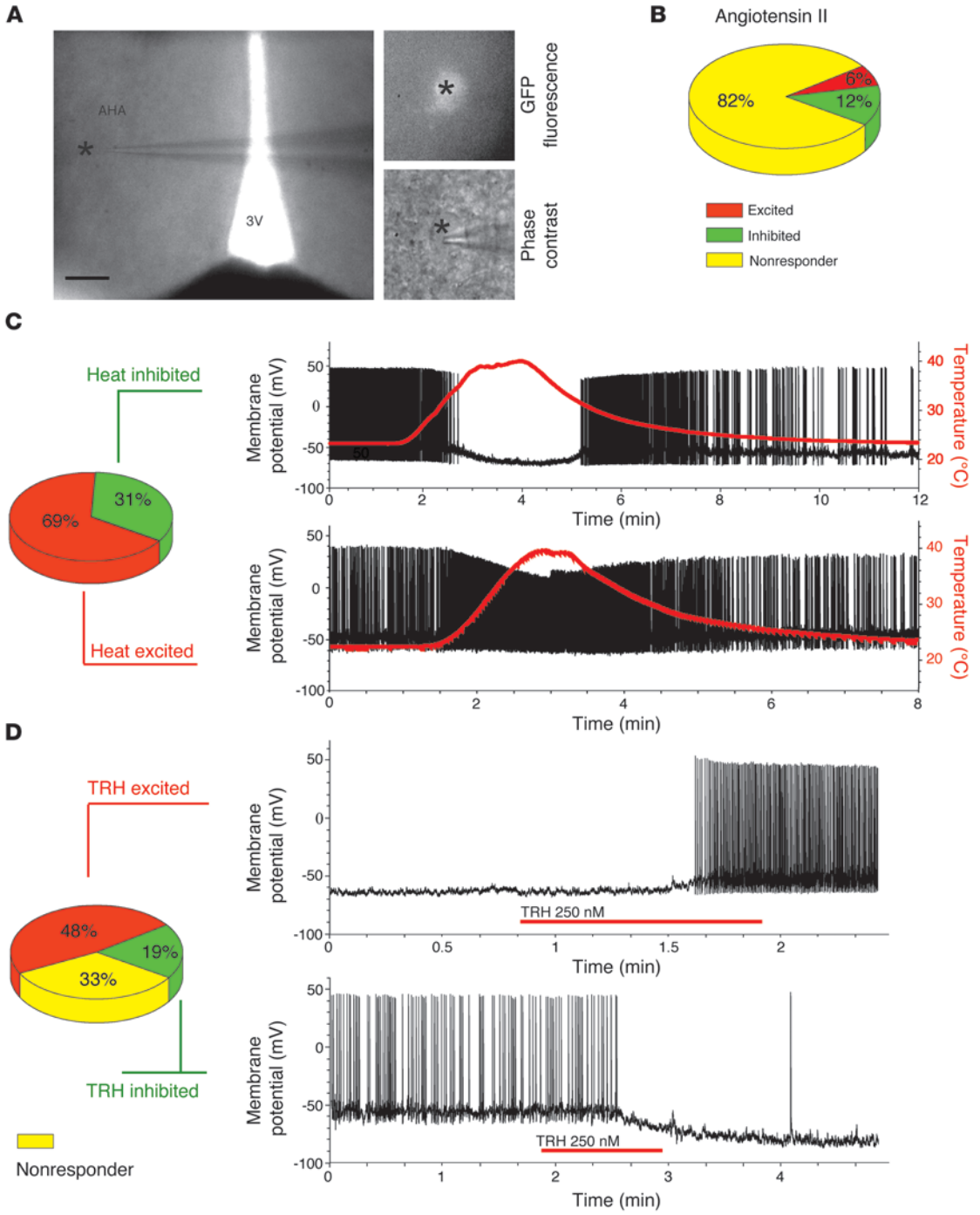

Figure 3
Electrophysiological responses of pv⁺ cells in the AHA. (**A**) Differential interference contrast (DIC) micrograph showing a recorded AHA pv⁺ neuron (indicated by an asterisk) (left; scale bar: 200 μm) and higher-magnification images of the same GFP-positive neuron under fluorescence and DIC (right; 500-fold magnification). (**B**) Response of AHA pv⁺ neurons to angiotensin II (82% no response; *n* = 14 out of 17). (**C**) Temperature responsiveness of the AHA pv⁺ cells to heat (31% inhibited, *n* = 5 out of 16, and 69% excited, *n* = 11 out of 16) in patch-clamp recordings on hypothalamic sections of transgenic pvGFP mice. (**D**) Response of AHA pv⁺ neurons to TRH (48% excited, *n* = 10 out of 21; 19% inhibited, *n* = 4 out of 21; and 33% nonresponsive, *n* = 7 out of 21) (the neuron in the top panel was held below threshold to prevent action potential firing; no holding current was applied in the other experiments).

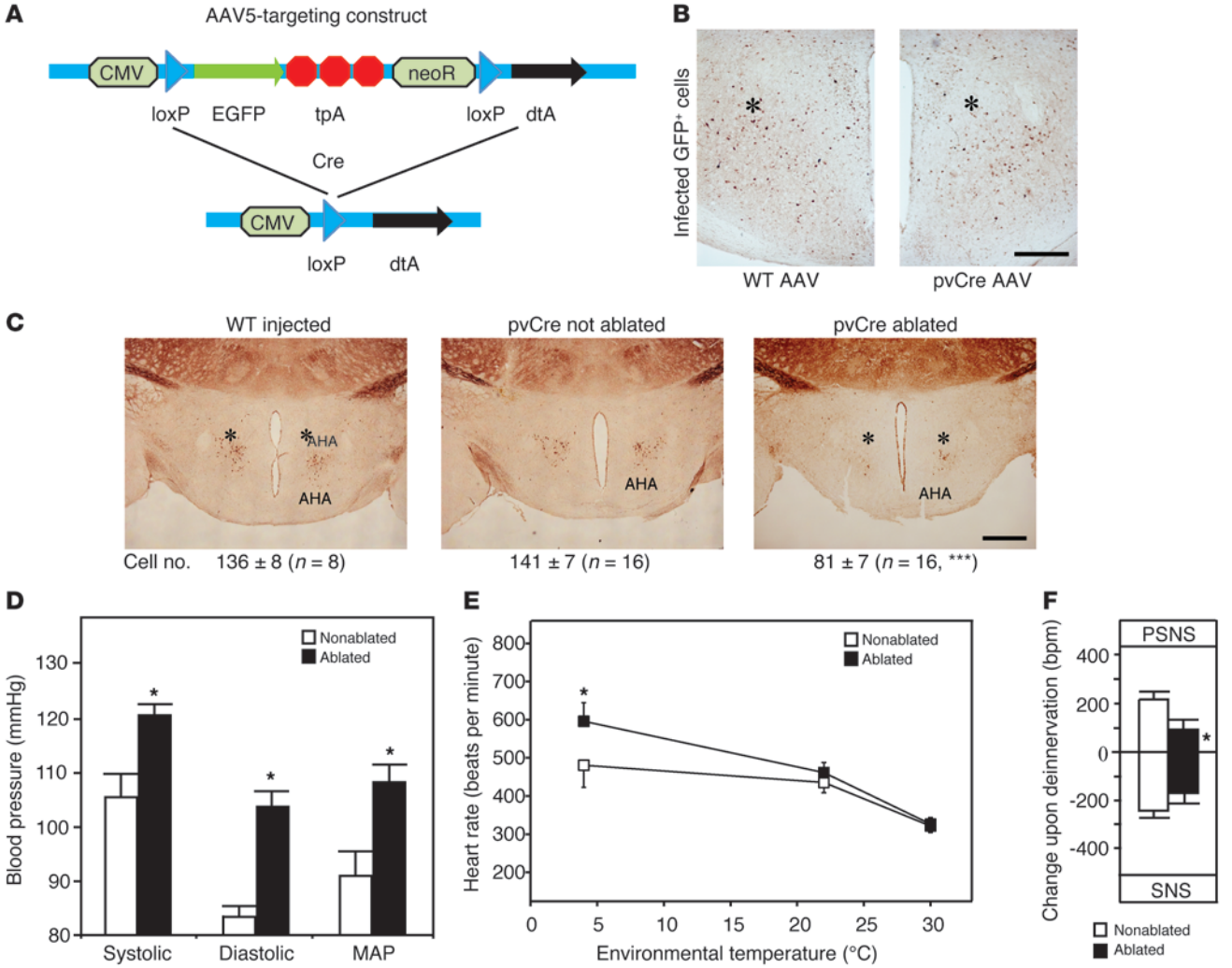

Figure 4

Effect of the in vivo ablation of AHA pv cells in pvCre mice. (**A**) AAV construct before and after Cre recombination. CMV, cytomegalovirus promotor; loxP, Cre recombination site; tpA, triple polyadenylation site; neoR, neomycin resistance gene; dtA, diphtheria toxin A. (**B**) Immunohistochemistry for EGFP at the site of the injection (indicated by asterisks) showing AAV-infected cells (scale bar: 250 μm). (**C**) Immunohistochemistry for pv in AAV-injected wild-type, nonablated pvCre, or AAV-injected ablated pvCre mice (the overall ablation efficiency is shown in the cell count at the bottom; ***$P < 0.001$ to nonablated, unpaired 2-tailed Student's t test; the respective groups for the subsequent cardiac and metabolic analyses had cell counts of 81 ± 13 in the ablated animals vs. 142 ± 10 in the nonablated animals; $n = 6$, $P = 0.002$; scale bar: 500 μm). Asterisks indicate the site of injection. (**D**) Systolic, diastolic, and mean arterial blood pressure in mice with reduced numbers of pv$^+$ cells in the AHA (black bars) and controls (white bars; *$P < 0.05$ for ablated vs. nonablated, unpaired 2-tailed Student's t test). (**E**) Heart rates in these mice (*$P < 0.05$ for ablated vs. nonablated at 4°C, 2-way ANOVA). (**F**) Change in heart rate upon pharmacological deinnervation of the parasympathetic nervous system (PSNS) (scopolamine methyl bromide) or the sympathetic nervous system (SNS) (timolol) in mice with reduced numbers of pv$^+$ cells in the AHA (black bars) and controls (white bars; *$P < 0.05$ for ablation, 2-way ANOVA). All values are mean ± SEM.

in animals with AHA pv$^+$ cell ablations (Figure 4D), with a 13% increase in systolic and a 22% increase in diastolic blood pressure. We did not observe any change in adrenal mRNA expression and aldosterone serum levels (Supplemental Figure 3J), serum angiotensin II levels (79% ± 18% of control levels, $P = 0.98$), or total T3 and thyroxine (T4) levels (total T3, 1.22 ± 0.18 nmol/l in control vs. 1.31 ± 0.28 nmol/l in ablated, $P = 0.63$; total T4, 46.25 ± 6.18 nmol/l in control vs. 46.20 ± 9.64 nmol/l in ablated, $P = 0.99$), suggesting that the AHA pv$^+$ cells control cardiovascular function directly by the autonomic nervous system rather than through endocrine alterations.

To understand the cardiovascular phenotype better, radio telemetry transmitters implanted into the abdominal cavity were used to measure heart rate in conscious and unrestrained animals. This revealed a minor tachycardia at room temperature in the animals with ablated AHA pv$^+$ cells, which was increased during night activity (Figure 4E and Supplemental Figure 3K). When exposed to cold, these mice exhibited a pronounced increase in heart rate, 24% higher than that in control animals (Figure 4E). Interestingly, the tachycardia disappeared entirely at thermoneutrality (Figure 4E).

Given the abnormal cardiovascular response to temperature and the fact that the autonomic innervation of the heart shifts in

rodents with decreasing temperature (26), we hypothesized that the ablation of AHA pv$^+$ cells changed the autonomic control of the cardiovascular system. To test this hypothesis, we performed a selective pharmacological deinnervation of the heart as described previously (12), using the muscarinic antagonist scopolamine methyl bromide and the β-adrenergic antagonist timolol (Supplemental Figure 3L). Indeed, the analysis revealed reduced sympathetic and parasympathetic input to the heart in mice with ablated AHA pv$^+$ cells (Figure 4F), demonstrating the important role of these neurons in the autonomic control of cardiovascular function.

Discussion

In this study we show that both thyroid hormone receptors are required for the development of a previously unknown population of parvalbuminergic cells in the anterior hypothalamus. Our data link for the first time to our knowledge defects in thyroid hormone signaling during development to a permanent cellular alteration in the hypothalamus. Moreover, as the cells are associated with the control of cardiovascular function, our study shows that developmental hypothyroidism may represent a previously unknown risk factor for cardiovascular disorders.

The anterior hypothalamus in blood pressure regulation and thermosensation. Already 50 years ago, anatomical studies by Folkow et al. demonstrated that electrolytic lesions in the AHA cause a dramatic increase in blood pressure, while electrical stimulation of the same region has the opposite effect (27). This connection between the anterior hypothalamus and autonomic regulation of blood pressure has been confirmed in subsequent studies (28–32). Thus, the data presented here provide information pertinent to understanding the mechanisms underlying the previously described role of the anterior hypothalamus in the autonomic control of cardiovascular functions. Since we did not observe alterations in brown fat thermogenesis in the ablation model, we conclude that the AHA pv$^+$ cells selectively control only a subset of autonomic functions, i.e., blood pressure and heart rate.

The integration of temperature information in the regulation of cardiovascular function has also been described previously for the anterior hypothalamus albeit only at the anatomical level (33). Our results now provide a distinct cellular connection between temperature sensation and cardiovascular function. Moreover, they are likely to facilitate further studies on thermosensation. Although the first thermosensitive neurons were described over 40 years ago (34, 35), and many attempts since then have been made to identify cellular markers (36), such cells are still only recognized by their electrophysiological responsiveness to temperature after random patch clamping. Using pv as biochemical marker for the thermosensitive neurons in the AHA, a reliable identification of a subgroup of these cells now becomes possible. Furthermore, it will allow cell-specific genetic manipulations of thermosensation and the central autonomic control of cardiovascular function.

Developmental hypothyroidism as novel risk factor for hypertension. Mice heterozygous for a point mutation in TRα1 represent an established animal model for receptor-mediated hypothyroidism (9, 11). Their adult phenotype is a combination of irreversible defects caused by the defective TRα1 signaling during brain development and impairments in acute TRα1 signaling (10, 12). However, as the acute impairments in TRα1 signaling can be reversed by treating the *Thra1*$^{+/m}$ mice with T3 (11), the identification of irreversible developmental defects becomes possible. In this study, we also observed overlapping developmental and acute defects in the regulation of blood pressure: the acutely reduced pulmonary *Ace* expression and serum angiotensin II levels were restored upon T3 treatment, and the hypertensive effect of the irreversibly reduced number of AHA pv$^+$ neurons was unmasked. That we observed a reduced number of AHA pv$^+$ neurons in mice lacking TRβ, exacerbated in *Thra1*$^{+/m}$*Thrb*$^{-/-}$ double mutants, demonstrates that the perinatal development of AHA pv$^+$ neurons critically depends on intact signaling by both TR isoforms. The precise molecular mechanisms by which TRs govern the development of these cells have yet to be elucidated; however, such an undertaking is complex due to the presence of at least 4 different AHA pv$^+$ subpopulations (based on their responses to temperature and TRH). Without reliable biochemical markers to differentiate these subpopulations, it cannot be established whether the different types of AHA pv$^+$ cells are similarly affected by defects in TRα or TRβ signaling. Consequently, the viral ablation model might not fully recapitulate the situation found in the TR mutant mice, as it targets all pv$^+$ cells similarly, whereas the mutant TR could theoretically perturb a subset. However, the hypertension was observed in the ablation model as well as the T3-treated *Thra1*$^{+/m}$ mice; thus, it is possible that any kind of developmental hypothyroidism or maternal hypothyroxinemia (37) could cause similar defects in the central regulation of cardiovascular function.

Consequences for patients. Several types of patients with genetic defects in thyroid hormone signaling have been identified during the past decade, including those with mutations in thyroid hormone transporters (38) and receptors (14, 39). In mice and humans, these defects often result in strongly impaired brain function. Thus, it would not be surprising if the central autonomic control were also affected in these patients. However, the first patient with a mutant TRα1 exhibited low blood pressure and did not present hypertension when treated with thyroxine (14) — a difference that is likely explained by the fact that her particular TRα1 mutation cannot be reactivated. Further analyses of the angiotensin system and the cardiovascular responses to temperature will be required in patients with TR mutations or defective thyroid hormone transporters to fully elucidate whether thyroid hormone exerts a similar role in the central control of cardiovascular function in humans.

In summary, our data emphasize the importance of thyroid hormone for cardiovascular function and brain development (40). With the discovery of the AHA pv$^+$ neurons, we are the first to our knowledge to identify a permanent cellular defect in the hypothalamus resulting from developmental hypothyroidism and add hypertension to the list of symptoms potentially arising from maternal hypothyroxinemia and/or congenital hypothyroidism.

Methods

Animals. The mouse strain expressing a chimeric TRα1-GFP protein to localize TRα1 expression was generated recently (41); *Thra1*$^{+/m}$ mice and crossings to TRβ-deficient mice were described in detail previously (11). The mice were backcrossed to C57BL/6NCr mice for 8 to 10 generations, and adult male mice were used for the experiments. For electrophysiological recordings, adult female heterozygous pvGFP mice were used (19). The stereotaxic ablations were performed in adult male heterozygous transgenic pvCre mice, obtained from The Jackson Laboratory (strain no. 008069) (42). Both strains were tested for correct transgene expression using immunohistochemistry or in situ hybridization histochemistry colocalization of GFP or Cre with pv. The animals were housed at 21°C on a 12-hour-light/12-hour-dark cycle with ad libitum access to food and water. If required, mice were treated with T3 via their drinking water with 0.01% albumin and 0.5 μg/ml T3 for 12 days. Food and water intake were recorded every 2 to 3 days over at least 2 weeks and averaged. Brown fat temperature was noninvasively recorded with an infrared camera (T335, FLIR Systems AB, 0.05°C sensitivity).

Metabolic and cardiovascular parameters. Implantable radio transmitters and receiver plates (Mini Mitter Respironics) were used to determine heart rate, body temperature, and activity of conscious and freely moving mice. The mice were anesthetized using isoflurane, and transmitters were implanted in the peritoneal cavity with the electrodes sutured to the right shoulder and the lower left chest. Subsequently, the animals were allowed to recover for 1 week before recordings. A baseline set was recorded for several days, including the determination of oxygen consumption, carbon dioxide production, and calculation of the respiratory quotient in metabolic cages with adjustable temperature settings (INCA metabolic system, Somedic). For the temperature experiments, mice were transferred during the daytime from 21°C to 4°C or 32°C, respectively, and their physiological responses were recorded over 3 hours. The pharmacological deinnervations with the peripherally active muscarinic antagonist scopolamine methyl bromide (Sigma-Aldrich, S8502-5G; 0.1 mg/kg) and the adrenergic β-blocker timolol maleate (Sigma-Aldrich, T6394-250MG; 1 mg/kg) were performed as described previously (12, 43). Blood pressure was recorded noninvasively with the tail-cuff–based SC1000 blood pressure analysis system (Hatteras). Serum levels of aldosterone and angiotensin II were determined using the ADI 900173 Aldosterone ELISA and ADI 900204 Angiotensin II ELISA Kits (Enzo Life Science). Total T3/T4 were determined using RIA test kits DSL-3100 and DSL-3200 (Diagnostic Products Corp.).

Immunohistochemistry. Immunohistochemistry was performed as described previously (17). The primary antibodies used were anti-pv (pv-25, Swant; 1:8,000), anti-calretinin (7699/4, Swant; 1:5,000), anti-calbindin (CB-38a, Swant; 1:5,000), anti-NeuN (MAB377, Millipore; 1:500), and anti-orexin (sc8070, Santa Cruz Biotechnology Inc.; 1:4,000) with species-specific biotinylated secondary antibodies (Vector Laboratories, Immunkemi; 1:250). For fluorescent immunohistochemistry, the primary antibodies against GFP (rabbit, ab290, abcam), TRPV4 (rabbit, ab39260, abcam), TRPM8 (rabbit, ab104569, abcam), and pv (mouse, no. 235, Swant) were used with Alexa Fluor 488 and Alexa Fluor 555 fluorophore-conjugated secondary antibodies (A31570 and A21206, Invitrogen).

For cell counting, consecutive sections from each brain, ranging from bregma 0.00 mm to –2.00 mm, were sampled in 5 tubes, with the sections in 1 tube covering intervals of 100 μm. At least 2 tubes per brain and 4 animals per genotype were stained for pv, positive cells in the AHA were bilaterally counted under the microscope, and the average was determined (with an average variation between 2 countings from the same animal of around 10%). Throughout, the raw cell count is given; for conversion to "true" cell number, the result needs to be multiplied by 2.85 (44).

Electrophysiology and whole-cell patch clamping. For electrophysiological experiments, pvGFP mice were decapitated. The brain was rapidly removed and placed in an ice-cold and oxygenated (95% O_2/5% CO_2) "cutting" solution containing 214 mM sucrose, 2.0 mM KCl, 1.2 mM NaH_2PO_4, 26 mM $NaHCO_3$, 1.3 mM $MgSO_4$, 2.4 mM $CaCl_2$, and 10 mM D-glucose. The brain was blocked and glued to a vibratome (Leica), where 225-μm-thick coronal sections of the hypothalamus containing the AHA were prepared. Slices were immediately transferred to a "recording" solution containing 127 mM NaCl, 2.0 mM KCl, 1.2 mM NaH_2PO_4, 26 mM $NaHCO_3$, 1.3 mM $MgCl_2$, 2.4 mM $CaCl_2$, and 10 mM D-glucose in a continuously oxygenated holding chamber at 35°C for a period of 25 minutes (45). Subsequently, slices were allowed to recover in "recording" solution at room temperature for a minimum of 2 hours before recording. For whole-cell recordings, slices were transferred to a submerged chamber and placed on an elevated grid that allows perfusion both above and below the slice. An Axioskop 2 FS Plus upright microscope (Carl Zeiss) was used for infrared differential interference contrast and fluorescence visualization of GFP-positive pv^+ cells. Whole-cell current clamp recordings were performed with pipettes (5–8 MΩ when filled with intracellular solution) made from borosilicate glass capillaries (World Precision Instruments) pulled on a P-97 Flaming/Brown micropipette puller (Sutter). The intracellular recording solution used in experiments contained 140 mM K-gluconate, 10 mM KCl, 10 mM HEPES, 1 mM EGTA, 2 mM Na_2ATP, pH 7.3 (with KOH). Recordings were performed using a Multiclamp 700B amplifier and pClamp9 software (Molecular Devices). Slow and fast capacitative components were automatically compensated for. Access resistance was monitored throughout the experiments, and only those cells with stable access resistance (changes <20%) were used for analysis. Liquid junction potential was not compensated. The recorded signals were sampled at 10 kHz and filtered at 2 kHz. During recording, slices were continuously perfused with oxygenated "recording" solution at a rate of ca. 4 ml/min. Perfusate temperature within the recording chamber was controlled and monitored using a TC-344B automatic temperature controller and an SH-27B inline heater (Both Warner Instruments). To investigate temperature sensitivity, no holding current was applied, the temperature of the perfusate in the recording chamber was reversibly ramped from 25°C to 40°C, and the subsequent membrane potential response of pv^+ neurons was recorded. For the calculation of membrane potential change or firing frequency, the biologically relevant range between 30°C and 40°C was used. This heating protocol was attempted once per slice. If indicated, the following drugs were applied through the extracellular solution: angiotensin (1 μM), tetrodotoxin (500 nM), tolbutamide (200 μM), and TRH (250 nM).

Stereotaxic ablation of Cre-positive neurons. Mice heterozygous for pvCre (strain no. 008069, The Jackson Laboratory — the construct inserts an IRES-Cre after the ORF of the pv gene) were anesthetized deeply and fixed in a frame for stereotaxic injections (Stoelting Instrument Co., AgnTho's). The position for the injection was determined with the stereotaxic frame to anterior-posterior coordinates of –0.75 mm and 0.5 mm lateral to each side (46), and 1 μl of the AAV (final concentration, 8×10^{12} viral genomes per ml, in phosphate-buffered saline with 5% glycerol and 6.5% mannitol, serotype AAV5; Vector Biolabs; containing the loxP-EGFP-STOP-loxP–diphtheria toxin A construct) (47) was injected with a Hamilton needle (701 N, ga 26S, 51 mm, pst 2, 10 μl, P/N 80366/00, tip cut at half; Hamilton) into the AHA at a depth of 5.0 mm. The virus was infused at a rate of 0.1 μl per 30 seconds, and the needle was slowly retracted after additional 5 minutes resting. The procedure was repeated on the other side. The animals were closely monitored for 2 weeks before the determination of physiological parameters or radiotelemetry surgery, which was done blinded, as the efficiency of the ablation was only determined postmortem by counting the pv^+ cells in the AHA. Animals with a cell count below 1 standard deviation from the average were considered "ablated," while sham-injected animals with an unaltered number of pv^+ cells were considered "nonablated." The overall ablation efficiency was 42% with 81 ± 7 cells (n = 16) in the ablated animals compared with 141 ± 7 cells in the nonablated animals (n = 16, $P < 0.001$; see Figure 4C); the respective groups for the radiotelemetry and metabolic experiments had cell counts of 81 ± 13 in the ablated and 142 ± 10 in the nonablated animals (n = 6, $P = 0.002$).

Real-time PCR. RNA was isolated from snap-frozen tissues using the RNeasy Mini Kit (Qiagen) according to the manufacturer's instructions. cDNA was generated using reverse transcription with Oligo-dT Primers (Invitrogen) and used for real-time PCR with the ABI 7300 system and the ABI Prism 7000 (Applied Biosystems). A standard curve was used to correct for PCR efficiency, and the results were normalized using *Hprt* as reference gene. An additional melting curve was recorded to confirm the specificity of the reaction. The primer sequences have been published previously (10) or are listed in Supplemental Table 1.

Statistics. All data are presented as mean ± SEM, unless stated otherwise. The P values were obtained by an unpaired 2-tailed Student's t test or a 2-way ANOVA followed by the Bonferroni post-hoc test when indicated. A P value of less than 0.05 was considered significant.

Study approval. Animal procedures were in accordance with European Community Council Directives and approved by Stockholm's Norra Djurförsöksetiska Nämnd (Stockholm, Sweden).

Acknowledgments

The authors thank Emelie Brinkhed and the personnel of our animal facilities for animal caretaking, Lilian Sundberg and Kristina Gottschling for technical assistance, Juan Pedro Martinez-Barbera for the dtA construct, Malin Kele and Jonas Frisén for support with stereotaxic injections, and Nina Balthasar for scientific discussion. This work was supported by the European Molecular Biology Organisation, the Deutsche Forschungsgemeinschaft, Thurings-stiftelse, Karolinska Institutets Stiftelse, and the American Thyroid Association (all to J. Mittag); Vetenskapsrådet (to J. Mittag, A. Arner, and B. Vennström); Karolinska Institutets EndoMet network (to C. Broberger and J. Mittag); the Swedish Cancer Society and Söderbergsstiftelse (to B. Vennström); the Swedish Heart Lung Foundation (to A. Arner) and Karolinska Institutets support for core facilities (to A. Arner); and The Netherlands Organization for Health Research and Development (grant no/ 916.86.020 to A. Alkemade) and the Ludgardine Bouwman Foundation (to A. Alkemade).

Received for publication June 8, 2012, and accepted in revised form October 18, 2012.

Address correspondence to: Björn Vennström, Department of Cell and Molecular Biology, Karolinska Institutet, P.O. Box 285, 17177 Stockholm, Sweden. Phone: 46.8.52487350; Fax: 46.8.348135; E-mail: bjorn.vennstrom@ki.se.

1. Magnus-Levy A. Uber den respiratorischen Gaswechsel unter dem Einfluss der Thyroidea sowie unter verschiedenen pathologischen Zustanden. *Berlin Klin Wochenschr*. 1895;34:650–652.
2. Klein I, Ojamaa K. Thyroid hormone and the cardiovascular system. *N Engl J Med*. 2001;344(7):501–509.
3. Kim B. Thyroid hormone as a determinant of energy expenditure and the basal metabolic rate. *Thyroid*. 2008;18(2):141–144.
4. Kahaly GJ, Dillmann WH. Thyroid hormone action in the heart. *Endocr Rev*. 2005;26(5):704–728.
5. Silva JE. Thermogenic mechanisms and their hormonal regulation. *Physiol Rev*. 2006;86(2):435–464.
6. Short KR, Nygren J, Barazzoni R, Levine J, Nair KS. T(3) increases mitochondrial ATP production in oxidative muscle despite increased expression of UCP2 and -3. *Am J Physiol Endocrinol Metab*. 2001; 280(5):E761–E769.
7. Fliers E, Klieverik LP, Kalsbeek A. Novel neural pathways for metabolic effects of thyroid hormone. *Trends Endocrinol Metab*. 2010;21(4):230–236.
8. Lopez M, et al. Hypothalamic AMPK and fatty acid metabolism mediate thyroid regulation of energy balance. *Nat Med*. 2010;16(9):1001–1008.
9. Vujovic M, et al. Interference of a mutant thyroid hormone receptor alpha1 with hepatic glucose metabolism. *Endocrinology*. 2009;150(6):2940–2947.
10. Sjogren M, et al. Hypermetabolism in mice caused by the central action of an unliganded thyroid hormone receptor alpha1. *EMBO J*. 2007; 26(21):4535–4545.
11. Tinnikov A, et al. Retardation of post-natal development caused by a negatively acting thyroid hormone receptor alpha1. *EMBO J*. 2002;21(19):5079–5087.
12. Mittag J, Davis B, Vujovic M, Arner A, Vennstrom B. Adaptations of the autonomous nervous system controlling heart rate are impaired by a mutant thyroid hormone receptor-alpha1. *Endocrinology*. 2010;151(5):2388–2395.
13. Warner A, Mittag J. Thyroid hormone and the central control of homeostasis. *J Mol Endocrinol*. 2012; 49(1):R29–R35.
14. Bochukova E, et al. A mutation in the thyroid hormone receptor alpha gene. *N Engl J Med*. 2012; 366(3):243–249.
15. Saper CB. The central autonomic nervous system: conscious visceral perception and autonomic pattern generation. *Annu Rev Neurosci*. 2002;25:433–469.
16. Mészár Z, Girard F, Saper CB, Celio MR. The lateral hypothalamic parvalbumin-immunoreactive (PV1) nucleus in rodents. *J Comp Neurol*. 2012; 520(4):798–815.
17. Wallis K, et al. Locomotor deficiencies and aberrant development of subtype-specific GABAergic interneurons caused by an unliganded thyroid hormone receptor alpha1. *J Neurosci*. 2008;28(8):1904–1915.
18. Forrest D, Erway LC, Ng L, Altschuler R, Curran T. Thyroid hormone receptor beta is essential for development of auditory function. *Nat Genet*. 1996; 13(3):354–357.
19. Meyer AH, Katona I, Blatow M, Rozov A, Monyer H. In vivo labeling of parvalbumin-positive interneurons and analysis of electrical coupling in identified neurons. *J Neurosci*. 2002;22(16):7055–7064.
20. Clapham DE, Miller C. A thermodynamic framework for understanding temperature sensing by transient receptor potential (TRP) channels. *Proc Natl Acad Sci U S A*. 2011;108(49):19492–19497.
21. Voets T, Talavera K, Owsianik G, Nilius B. Sensing with TRP channels. *Nat Chem Biol*. 2005;1(2):85–92.
22. McCoy DD, Knowlton WM, McKemy DD. Scraping through the ice: uncovering the role of TRPM8 in cold transduction. *Am J Physiol Regul Integr Comp Physiol*. 2011;300(6):R1278–R1287.
23. Shinozuka K, Shimoura K, Hattori K. Effects of thyrotropin-releasing hormone and its analogue, NS-3, on blood pressure, heart rate, and serum catecholamine levels in rats. *Gen Pharmacol*. 1997; 28(2):209–214.
24. Knight WD, Swoap SJ, Parsons AD, Overton JM. Central thyrotropin-releasing hormone infusion opposes cardiovascular and metabolic suppression during caloric restriction. *Neuroendocrinology*. 2006; 83(2):69–76.
25. Huang XC, Saigusa T, Iriki M. Comparison of TRH and its analog (NS-3) in thermoregulatory and cardiovascular effects. *Peptides*. 1992;13(2):305–311.
26. Swoap SJ, Li C, Wess J, Parsons AD, Williams TD, Overton JM. Vagal tone dominates autonomic control of mouse heart rate at thermoneutrality. *Am J Physiol Heart Circ Physiol*. 2008;294(4):H1581–H1588.
27. Folkow B, Johansson B, Oberg B. A hypothalamic structure with a marked inhibitory effect on tonic sympathetic activity. *Acta Physiol Scand*. 1959; 47:262–270.
28. Yilmaz MS, Millington WR, Feleder C. The preoptic anterior hypothalamic area mediates initiation of the hypotensive response induced by LPS in male rats. *Shock*. 2008;29(2):232–237.
29. Villanueva A, et al. Central cannabinoid 1 receptor antagonist administration prevents endotoxic hypotension affecting norepinephrine release in the preoptic anterior hypothalamic area. *Shock*. 2009; 32(6):614–620.
30. Hagiwara Y, Kubo T. Anterior hypothalamic neurons respond to blood pressure changes via gamma-aminobutyric acid and angiotensins in rats. *Neurosci Lett*. 2005;384(3):250–253.
31. Mayer MA, et al. Role of hypothalamic alpha-adrenoceptor activity in fructose-induced hypertension. *Clin Exp Pharmacol Physiol*. 2006; 33(10):904–909.
32. Hagiwara Y, Sasaki Y, Fukumori R, Kubo T. Central injection of hypertonic saline activates angiotensin II-sensitive neurons in the anterior hypothalamic area of rats. *Brain Res*. 2005;1046(1–2):165–171.
33. Folkow B, Strom G, Uvnas B. Cutaneous vasodilatation elicited by local heating of the anterior hypothalamus in cats and dogs. *Acta Physiol Scand*. 1949; 17(4):317–326.
34. Nakayama T, Suzuki M, Ishizuka N. Action of progesterone on preoptic thermosensitive neurones. *Nature*. 1975;258(5530):80.
35. Beckman AL, Eisenman JS. Microelectrophoresis of biogenic amines on hypothalamic thermosensitive cells. *Science*. 1970;170(3955):334–336.
36. Eberwine J, Bartfai T. Single cell transcriptomics of hypothalamic warm sensitive neurons that control core body temperature and fever response Signaling asymmetry and an extension of chemical neuroanatomy. *Pharmacol Ther*. 2011; 129(3):241–259.
37. de Escobar GM, Obregon MJ, del Rey FE. Maternal thyroid hormones early in pregnancy and fetal brain development. *Best Pract Res Clin Endocrinol Metab*. 2004;18(2):225–248.
38. Friesema EC, et al. Association between mutations in a thyroid hormone transporter and severe X-linked psychomotor retardation. *Lancet*. 2004; 364(9443):1435–1437.
39. van Mullem A, et al. Clinical phenotype and mutant TRalpha1. *N Engl J Med*. 2012;366(15):1451–1453.
40. Bernal J. Thyroid hormone receptors in brain development and function. *Nat Clin Pract Endocrinol Metab*. 2007;3(3):249–259.
41. Wallis K, Dudazy S, van Hogerlinden M, Nordstrom K, Mittag J, Vennstrom B. The thyroid hormone receptor alpha1 protein is expressed in embryonic postmitotic neurons and persists in most adult neurons. *Mol Endocrinol*. 2010; 24(10):1904–1916.
42. Hippenmeyer S, et al. A developmental switch in the response of DRG neurons to ETS transcription factor signaling. *PLoS Biol*. 2005;3(5):e159.
43. Johnson Rowsey P, Yang YL, Gordon CJ. Peripheral cholinergic pathway modulates hyperthermia induced by stress in rats exposed to open-field stress. *J Appl Physiol*. 2002;92(2):789–794.
44. Guillery RW, Herrup K. Quantification without pontification: choosing a method for counting objects in sectioned tissues. *J Comp Neurol*. 1997; 386(1):2–7.
45. Lyons DJ, Horjales-Araujo E, Broberger C. Synchronized network oscillations in rat tuberoinfundibular dopamine neurons: switch to tonic discharge by thyrotropin-releasing hormone. *Neuron*. 2011;65(2):217–229.
46. Franklin KBJ, Paxinos G. *The Mouse Brain in Stereotaxic Coordinates*. San Diego, California, USA: Academic Press; 1997.
47. Ivanova A, Signore M, Caro N, Greene ND, Copp AJ, Martinez-Barbera JP. In vivo genetic ablation by Cre-mediated expression of diphtheria toxin fragment A. *Genesis*. 2005;43(3):129–135.